Journal of Hydrology 612 (2022) 128230

Contents lists available at ScienceDirect

Journal of Hydrology

journal homepage: www.elsevier.com/locate/jhydrol

Research papers

White pine blister rust, logging, and species replacement increased streamflow in a montane watershed in the northern Rockies, USA

Liang Wei [a,b,1,*], Hang Zhou [c,1], Andrew T. Hudak [d], Timothy E. Link [b], Adrienne Marshall [b,e], Katy L. Kavanagh [f], John T. Abatzoglou [c,g], Theresa B. Jain [d], John C. Byrne [d], Robert Denner [d], Patrick A. Fekety [h], Jonathan Sandquist [d], Xizi Yu [a], John D. Marshall [i]

[a] MOE Key Laboratory of Western China's Environmental System, College of Earth and Environmental Sciences, Lanzhou University, Lanzhou, Gansu 730000, China
[b] Department of Forest, Rangeland, and Fire Sciences, University of Idaho, Moscow, ID 83844, USA
[c] Department of Geography, University of Idaho, Moscow, ID 83844, USA
[d] Rocky Mountain Research Station, USDA Forest Service, Moscow, ID 83843, USA
[e] Hydrologic Sciences and Engineering Program, Colorado School of Mines, Golden, CO 80401, USA
[f] College of Forestry, Oregon State University Corvallis, OR 97331-5704, USA
[g] Management of Complex Systems, University of California, Merced, Merced, CA 95343, USA
[h] Natural Resources Ecology Laboratory, Colorado State University, Fort Collins, CO 80523, USA
[i] Department of Forest Ecology and Management, Swedish University of Agricultural Sciences, Skogmarksgränd, Umeå 90736, Sweden

ARTICLE INFO

Keywords:
Vegetation change
Western white pine mortality
Long-term hydrology data
SHAW model
Forest disturbance
Ecohydrology

ABSTRACT

Vegetation changes can strongly influence the hydrological cycle, including streamflow, but the effects of plant diseases have seldom been described. In the mid-20th century, the invasion of an exotic disease, white pine blister rust, precipitated widespread mortality of western white pine (WWP; *Pinus monticola* Dougl.) in the northern Rocky Mountains, USA. These events converted a forest dominated by white pine into one dominated by more shade-tolerant tree species. The long-term hydrological implications of this historical shift in forest composition have not been adequately explored, in part because collocated long-term vegetation, meteorology, and hydrology data are rare. We assembled long-term streamflow, climate, and vegetation records for a small (4.0 km^2) forested watershed in the U.S. northern Rocky Mountains. We used a minimally-calibrated, physically-based model to simulate historical changes in the water budget based on observed vegetation changes along with the historical climate. The observed hydrological anomalies were attributed to a combination of white pine blister rust induced tree mortality, harvest, and eventual species replacement. Small increases in streamflow began in the basin in the 1940s, when the basal area of WWP began to decrease. More dramatic increases in streamflow started after harvesting began in 1966. Based on both observations and modeling, streamflow increased by ~131–179 mm between the 1940s and the 2000s (30–40% of the 2000s' streamflow) in contrast to documented regional streamflow declines. Approximately 1/3 of the flow changes were attributed to blister rust and 2/3 to harvest, as shade-tolerant species instead of WWP regenerated in response to both. This study highlights the importance of long-term ecohydrological data, which made it possible to detect the influence of the invasion of an exotic pathogen against a backdrop of periodic timber harvest. It also showed that the species replacement after these disturbances caused long-term changes in the flow regime, providing a clear and relevant example of how land cover changes can affect interannual hydrological dynamics.

1. Introduction

Forests play a crucial role in water cycling by returning a large amount of water into the atmosphere through evapotranspiration (ET). Changes in forests alter water cycling mainly by changing canopy interception and transpiration (Whitehead and Robinson, 1993) and

* Corresponding author at: MOE Key Laboratory of Western China's Environmental System, College of Earth and Environmental Sciences, Lanzhou University, Lanzhou, Gansu 730000, China.
E-mail address: liangwei@alumni.uidaho.edu (L. Wei).
[1] Authors contributed equally to this work.

https://doi.org/10.1016/j.jhydrol.2022.128230
Received 22 November 2021; Received in revised form 21 May 2022; Accepted 14 July 2022
Available online 21 July 2022
0022-1694/© 2022 Elsevier B.V. All rights reserved.

snow dynamics in seasonally cold climates (Varhola et al., 2010). There is a long history of quantification of changes in streamflow in response to forest harvesting (Andréassian, 2004; Brown et al., 2005; Buttle, 2011; Picchio et al., 2021; Stednick, 1996). More recently, streamflow responses have been detected in response to fire (Seibert et al., 2010) and, in one case, a foliar disease (Bladon et al., 2019); bark beetle attacks did not significantly change streamflow hydrology (Slinski et al., 2016). Recent reviews of this literature have raised questions about the generality of flow increases following forest disturbance and underscore the importance of evaluating disturbance effects on hydrological processes (Goeking and Tarboton, 2020). This calls for a more nuanced understanding of the role of vegetation in controlling water yield, including the role of subsurface storage (McDonnell et al., 2018), forest age (e.g. Teuling and Hoek van Dijke, 2020), species change (e.g. Swank and Douglass, 1974; Swank and Miner, 1968) and diversity of forest conditions within a watershed (Coble et al., 2020).

In this context, the historical mortality of western white pine (WWP; *Pinus monticola* Dougl. Ex D. Don) in the early 20th century in the Pacific Northwest USA serves as an informative example of dramatic vegetation change and its impact on water cycling (Tinkham et al., 2015). WWP was prevalent throughout the northern Rocky Mountains on all aspects and slopes and was resistant to endemic disturbances (Jain and Graham, 2005). Between 1900 and 1992, the WWP-dominated area in northern Idaho declined from about 8000 km^2 to merely 47 km^2 (Fig. S1) (Fins et al., 2002; Harvey et al., 2008; Neuenschwander, et al., 1999). The mortality had multiple causes, including widespread logging beginning in the late 19th century (Neuenschwander, et al., 1999; Strong and Webb, 1970) and an extensive high severity fire in northern Idaho (the "Big Burn") in 1910 (Fig. S1) (Diaz and Swetnam, 2013; Egan, 2009; Plummer, 1912). WWP mortality on an even larger scale occurred after 1910 due to an exotic disease lethal to WWP. The disease, white pine blister rust, is caused by the fungus *Cronartium ribicola*, native to Asia, and accidentally introduced by timber importers from Europe to British Columbia; it subsequently spread to northern Idaho in the 1920s (Harvey et al., 2008; Neuenschwander, et al., 1999). White pine blister rust not only killed most adult trees, but also dramatically reduced the survival of WWP seedlings and hence inhibited regeneration (Tomback and Achuff, 2010). Despite efforts to control the spread of blister rust and breeding of rust-resistant seedlings, WWP mortality accelerated in the 1950s in northern Idaho, and the species has yet to recover to the point of stand dominance (Neuenschwander, et al., 1999) unless planted and carefully managed (Schnepf and Schwandt, 2006).

A new ecological and hydrological regime may have started in this forest ecosystem with the gradual replacement of WWP by shade-tolerant species, namely: western redcedar (*Thuja plicata* Donn ex D. Don), western hemlock (*Tsuga heterophylla* (Raf.) Sarg.), and grand fir (*Abies grandis* (Dougl. ex D. Don) Lindl.). These shade-tolerant species transpire approximately half the water relative to WWP per unit leaf area, reflected in highly different stomatal limits on transpiration (Pangle et al., 2015). Due to such a large difference in transpiration, the high initial cover of WWP, and the magnitude of WWP mortality, WWP mortality is expected to decrease transpiration with concomitant increases in streamflow. This may cause a slower hydrological response than from relatively sudden disturbances such as forest harvest, wildfire, and insect outbreaks that have been more widely investigated.

Despite the widespread replacement of WWP by shade-tolerant species in the interior U.S. Northwest and possible impacts on water cycling, such historical impacts on water budgets have not been quantitatively assessed with either observations or modeling. In this case, modeling facilitates disentangling the hydrologic processes due to climate and vegetation changes that result in net changes in streamflow. A rare opportunity was found in a data-rich small watershed in an experimental forest in northern Idaho where WWP vegetation was gradually replaced by shade-tolerant tree species. The watershed was excluded from widespread commercial WWP logging and fire impacts in the early 20th century. Some small-scale harvests did happen after the early 20th century, but detailed harvest records were uncovered and compiled. Streamflow and climatic data were systematically monitored prior to shifts in species composition within the watershed (Link et al., 2015; Tinkham et al., 2015). Because of the valuable historical records, this study serves as a novel example to assess and parse the hydrological impacts of shifts in forest cover type due to introduced blister rust and limited timber harvest.

We hypothesized that a significant increase in streamflow should have occurred due to WWP mortality and small-scale timber harvest, due to the large difference in water consumption between historical WWP-dominant and current shade-tolerant forests. The specific objective of this research is to quantify long-term differences in observed streamflows that are specifically attributed to species changes from gradual pathogen-induced mortality versus vegetation changes from discrete harvests. Although a paired-catchment experiment would be the most effective approach to reveal such impacts, this option was not available since no watersheds with WWP vegetation unimpacted by blister rust remained. Therefore, this study employed a multi-decadal data record and physically-based hydrological model to test the hypothesis by quantitatively estimating changes in transpiration, streamflow, and soil moisture due to hydroclimatic and vegetation changes in the basin over 70 years. The model was previously parameterized for this watershed (Wei et al 2016). A wealth of long-term onsite observational data facilitated the analysis and modeling, including climate, snow depth, streamflow, forest cover and inventory, and management history.

2. Methods

2.1. Study area

The Priest River Experimental Forest (PREF; 25.8 km^2), established in 1911 (Wellner, 1976), is located in the panhandle of northern Idaho (48°45′N, 116°49′W), which is in the continental/maritime hydroclimatic region of the United States. The annual mean temperature is ~ 6.7 °C and the annual mean precipitation is 808 mm at PREF headquarters (726 m above sea level; National Climatic Data Center (NCDC), station No: USC00107386 from 1930 to 2011; Fig. 1). Approximately 65% of the annual precipitation occurred from November to April (Fig. 2). Within PREF, annual mean precipitation varies with orographic enhancement between 812 mm yr^{-1} at low elevations (675 m) to 1270 mm yr^{-1} at higher elevations (1825 m) (Pangle et al., 2015). Soils at PREF are loamy Inceptisols with a 10–20 cm deep volcanic ash cap at the top of the mineral soil (Berryman et al., 2014), and the bedrock is metamorphic rocks comprised of gneiss and schists (the U.S. General Soil Map (STATSGO2), c.f. Srivastava et al., 2020).

PREF has long-term records for forest composition, hydrometeorology, and streamflow. A gauging station (Benton Dam) has recorded streamflow since 1939 for the Upper Benton Basin (UBB), a small (4.0 km^2; 400 ha) watershed which ranges from 805 to 1700 m in elevation (Fig. 1). These observational data were mainly used for driving the process-based model to assess water balance changes resulting from vegetation dynamics (see 2.5 and 2.6).

Forest disturbances in UBB were recorded since the establishment of PREF. There were two reports of fires in UBB since the inception of PREF in 1911. In 1967, there was a prescribed fire that burned 16–20 ha. In August 2008, a small fire burned 2.8 ha before it was quickly extinguished, on the southern boundary of PREF and mostly outside the ridgeline that delineates the UBB drainage. The earliest records of harvest activity were neither accurately mapped within UBB nor labeled as to the type of cut, but based on available records and given logging practices at that time were most likely selective cuts of ~8.1 ha in 1924–1926 and ~36.4 ha in 1939. In 1941 a 91 m × 1336 m strip (32.4 ha) running N-S was clearcut across the entire UBB in an early forestry study. These harvest events were considered as part of the background condition for purposes of this study beginning in 1941, because we used

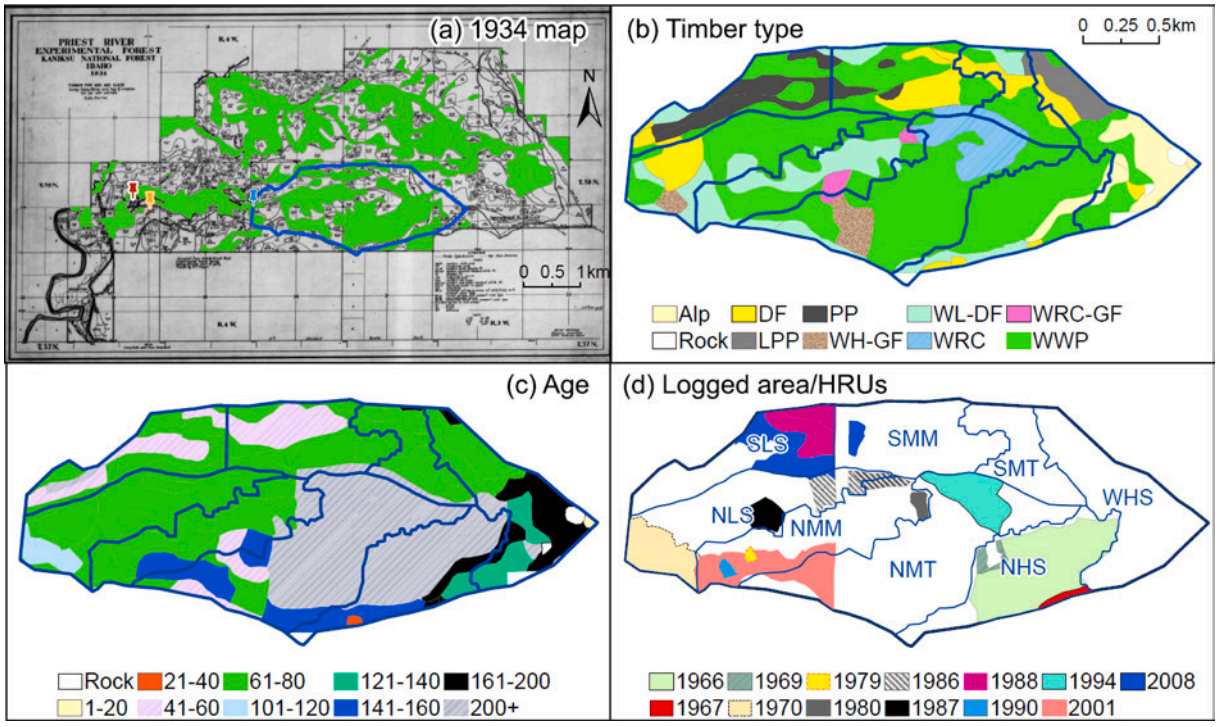

Fig. 1. Historical vegetation (a-c) and 21 hydrological response units (HRUs) (d) of the study area. A 1934 timber type map of PREF (a) was digitized; the information for timber type (b) and tree age (c; in years) of Upper Benton Basin (UBB, blue boundary in Fig. a) in 1934 were obtained from the map. Western white pine was the most abundant timber type (green) in 1934 in PREF based on a digitized stand map attributed with timber type and age class information (a). About 35% and 41% of the land area was WWP timber type (green) inside PREF and UBB, respectively. UBB was previously divided into eight HRUs in Wei et al. (2016) (blue boundary in b-d and three-letter names in d; marked with 3-letter acronyms; see also Table S1); 13 more HRUs to represent logging events (marked with logged years; Table S2) were separated from eight original HRUs in this study (d). Pins in Fig. a show the gauging station (Benton Dam; blue pin), Headquarters (red), and Benton Meadow (orange). Timber type acronyms in Fig. b: Alp, subalpine forest; DF, Douglas-fir; PP, ponderosa pine; WL, western larch; WRC, western redcedar; GF, grand fir; LPP, lodgepole pine; WWP, western white pine.

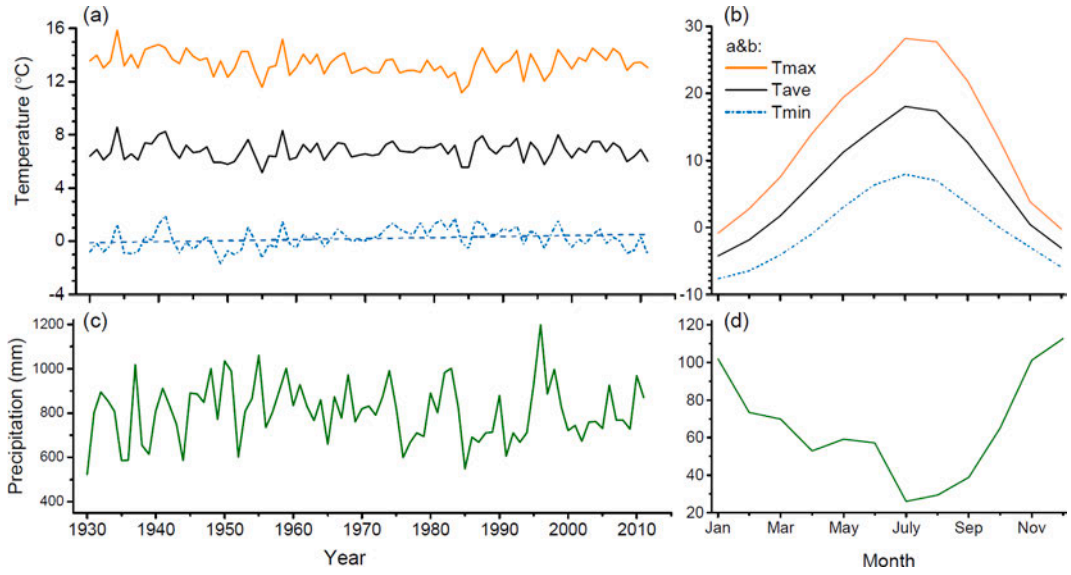

Fig. 2. Annual and monthly temperatures (a, b) and precipitation (c, d) in PREF from 1930 to 2011 at PREF Headquarters. The annual mean daily minimum temperature (T_{min}) had a significant increase (Mann-Kendall analysis, p = 0.02, Sen's slope = 0.0096; Fig. a). The Blue dotted line in (a) indicates significant linear regressions (P < 0.05) for visual estimation of trends. Annual mean daily average (T_{max}) and maximum (T_{max}) temperature (a), and precipitation (c) did not significantly change. The majority of precipitation occurs in cold months while precipitation in warm summer months is low (c & d). (For interpretation of the references to colour in this figure legend, the reader is referred to the web version of this article.)

the 1940s as a calibration period (see 2.6 for detail).

There were 13 records of small experimental timber harvests in UBB in 13 years from 1966 to 2010 (Table S2). Most of the harvested areas were clearcuts followed by natural regeneration. Tree replanting in UBB was limited to 16 ha in 1990 (ponderosa pine and western white pine) and 2 ha in 2007 (ponderosa pine, western white pine, western larch).

The fraction of land area harvested in each entry ranged from 0.9 ha (0.2%) to 36 ha (9.0%) (mean = 2.3%); such a small percentage of area harvested per entry is expected to have a minor, short-term effect on streamflow (Stednick, 1996), but cumulatively may produce larger effects. We therefore estimated the impact of harvests with the physically-based model (see 2.6) to deconvolve the interacting effects of forest harvest, regeneration, and WWP mortality on streamflow.

Forests at PREF and UBB contained therein were historically dominated by WWP (Fig. 1) before the 1950s (Tinkham et al., 2015) and are currently dominated by shade-tolerant conifer species (Fig. 3). Five major shade-tolerant tree species (western hemlock, western redcedar, subalpine fir, Engelmann spruce, and grand fir) comprise 60.0% of the current basal area, while intermediate shade-tolerant Douglas-fir and WWP comprised 20.3% and 2.9%, respectively, of current basal area (Duursma et al., 2003) (Fig. 3). In addition to lower transpiration and productivity relative to WWP (Pangle et al., 2015), shade-tolerant species are susceptible to native root diseases (e.g., laminated root disease, *Armillaria* root disease, brown cubical rot, and butt rot), while pine species are normally tolerant to them (Neuenschwander, et al., 1999). Therefore, the new forest types are more susceptible to native root diseases, which may further reduce forest productivity and evapotranspiration (Cruickshank et al., 2011; Lockman et al., 2016) and further contribute to increased streamflow.

2.2. Vegetation change

We estimated the vegetation changes based on a network of permanent plots in PREF which have been maintained since as early as 1914. There were 25 permanent plots in total; we used plots with >60 years of records (n = 21; Fig. S2 and Fig. 4). Plots were measured every 5–10 years to document forest growth and yield. During each measurement campaign, tree species were recorded and DBH was measured. We used these data to quantify changes in basal area and tree species composition. As the measurements were conducted in different years across plots (Fig. S2), we averaged the data by decade to facilitate comparison through time.

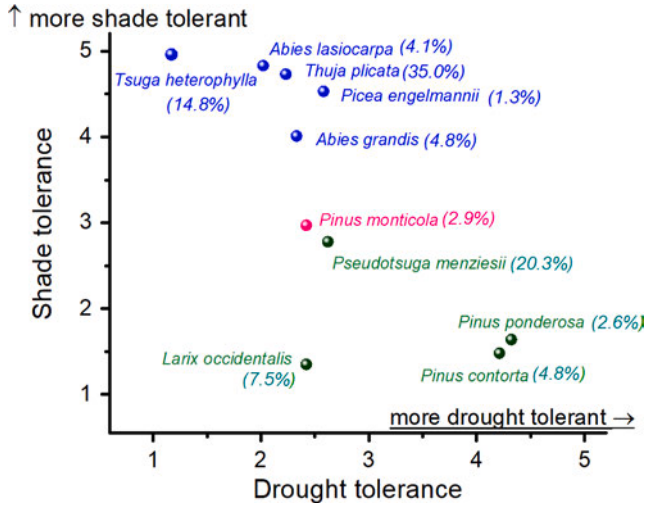

Fig. 3. Composition of current (2000s) shade-tolerant forest in PREF based on observed basal area. Percentage numbers indicate the composition of each species in basal area in PREF based on Duursma et al. (2003). Shade- and drought-tolerant information are obtained from Niinemets and Valladares (2006) and Wei et al. (2019); 1 indicates very intolerant and 5 very tolerant. Historically dominant Western White Pine (WWP; pink symbol) comprised only 2.9% of basal area in the 2000s, while shade-tolerant species (blue symbols; shade tolerance ≥ 4) comprised 60.0%. Current forests have similar drought tolerance but more shade-tolerant species than historical WWP dominant forests. Tree species: western white pine (*Pinus monticola*), western hemlock (*Tsuga heterophylla*), subalpine fir (*Abies lasiocarpa*), western redcedar (*Thuja plicata*), Engelmann spruce (*Picea engelmannii*), grand fir (*Abies grandis*), Douglas-fir (*Pseudotsuga menziesii*), western larch (*Larix occidentalis*), ponderosa pine (*Pinus ponderosa*), and lodgepole pine (*Pinus contorta*), (For interpretation of the references to colour in this figure legend, the reader is referred to the web version of this article.)

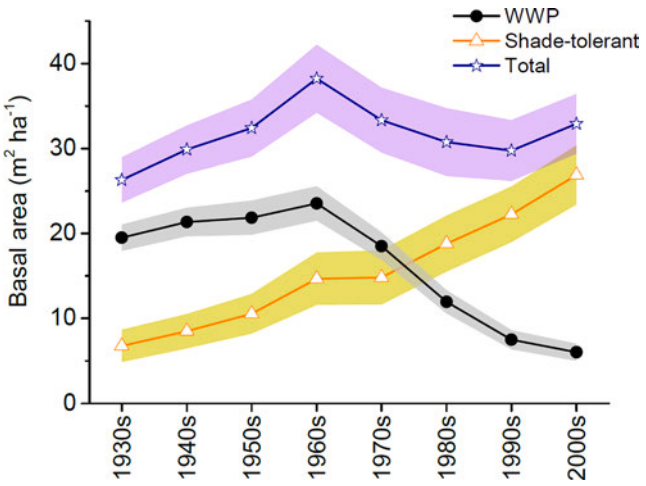

Fig. 4. Historical changes in observed mean basal area of living trees at 21 unharvested permanent plots in PREF. Individual figures for each plot can be found in Fig. S2. The mean basal area of WWP started decreasing after the 1960s while the mean basal area of shade-tolerant species (western redcedar, western hemlock, and grand fir) increased through time. Data were averaged for 21 plots from the 1930s to the 1990s and from 19 plots in the 2000s (two plots had no measurements in the 2000s). Shaded areas show standard errors.

Water balance simulations with the Simultaneous Heat and Water (SHAW) model (see 2.5 and 2.6 for more detail) required stand properties (i.e., leaf area index (LAI), aboveground biomass, and vegetation height) as inputs, but the historical observations were lacking. Therefore, we used the observed basal area information of permanent plots to inform LAI, aboveground biomass, and vegetation height for the model parameterization. Specifically, we used modeled forest growth for a very similar shade-tolerant forest in northern Idaho (Wei et al., 2014; Wei et al., 2018) as a reference and cross-referenced LAI, biomass, and vegetation height information with observed basal area in PREF (Fig. S3). The widely used forest growth model, Physiological Processes Predicting Growth (3-PG; Landsberg and Waring, 1997) was used to derive key canopy parameters for different age classes. The modeled forest growth was well calibrated and validated with observed stand properties, transpiration, and stable carbon isotope data (Wei et al., 2014). Moreover, the simulation started from a new regenerating forest post-harvest and hence represented a similar growth condition to the regeneration of forests at PREF after harvest.

2.3. Streamflow and snow observations

Streamflow has been recorded at Benton Dam with two trapezoidal Cipolletti weirs since 1939 (Stage, 1957). Water flows through only the smaller weir with a 1-foot (0.3048 m) crest at low flow, and through both the smaller and the larger weir with a 10-foot crest when the head exceeds 0.75 feet. The water level is recorded in a stilling well connected to a pond above the dam (Stage, 1957). Different equipment and media were used to record the data throughout the historical period ranging from mechanical strip charts to electronic water level sensors connected to electronic data loggers; data were presented in a variety of formats ranging from undigitized strip charts, digitized printed records, and various electronic formats (Link et al., 2015; Stage, 1957; Wei et al., 2016). Data from different equipment and media were error-checked and cross-compared for quality control; all quality-controlled streamflow data and metadata were compiled into a common electronic format

for a digital archive which is publicly available (Link et al., 2015).

Snow depth and snow water equivalent (SWE) were recorded in PREF. Daily snow depth data were measured at the Headquarters since 1911 (725 m a.s.l; NCDC: USC00107386). Monthly snow depth and SWE data were measured at Benton Meadow station (725 m a.s.l) since 1936 (Natural Resources Conservation Service). The Headquarters and Benton Meadow sites are in close proximity downstream and west of UBB (Fig. 1).

2.4. Historical hydrometeorological data

To drive the model, we used observed and estimated hydrometeorological data from 1930 to 2010, which included daily maximum and minimum temperatures (T_{max}, T_{min}), precipitation, shortwave radiation, relative humidity, and wind speed. Details about historical hydrometeorological data can be found in the online supplementary materials.

2.5. Water budget simulations

We used a physically-based hydrological model with multi-layer vegetation, the Simultaneous Heat and Water (SHAW) model (Flerchinger et al., 1990; Flerchinger et al., 1998; Flerchinger et al., 1996; Link et al., 2004), to simulate the water budget in the UBB. SHAW is a one-dimensional model based on fundamental physical hydrological processes. It simulates the transfer of heat, liquid water, and water vapor through a plant-snow-residue-soil system on a user-selected time step ranging from hourly to daily (daily in this study). It includes major hydrological processes: precipitation, snowpack development and ablation, evaporation, transpiration, infiltration and soil moisture redistribution, deep percolation, and runoff. Detailed descriptions of the model can be found in previous publications (Chauvin et al., 2011; Flerchinger et al., 1998; Flerchinger et al., 1996; Link et al., 2004). We simulated the water budget of the UBB in each HRU to estimate potential differences between current shade-tolerant and historical WWP dominated vegetation and to compare the results to observed streamflows. The water budget of a watershed can be written as:

$$P = E + Tr + Q + \Delta S \tag{1}$$

where P = precipitation, E = evaporation + sublimation, Tr = transpiration, Q = streamflow, and ΔS = changes in soil water storage (all in mm year^{-1}). All these components are directly simulated in the SHAW model except streamflow which we assume is equal to the sum of simulated deep percolation and surface runoff for annual water balance estimates assuming negligible amounts of deep seepage. This is a reasonable assumption for the UBB because it is a steep watershed with shallow soil overlaying highly impermeable bedrock (Cline et al., 1977). Therefore, deep percolation is expected to rapidly convert to streamflow. This approach was shown to be effective for quantifying the annual water balance at UBB (Wei et al., 2016); by calibrating the transpiration but not streamflow, the model reasonably simulated streamflow without systematic errors. The successful simulation of streamflow without calibration also corroborated the expectation that deep percolation was minimal.

Vegetation dynamics used as inputs to SHAW have direct impacts on the simulated water budget. LAI describes the amount of transpiring surface in the model; an increase in LAI typically increases transpiration and precipitation interception, but also decreases soil evaporation due to increased radiation interception. Vegetation height has offsetting impacts on evapotranspiration: increased vegetation height increases surface roughness and therefore turbulent transfer from the top of the canopy; it also impedes water vapor transport from leaves and the soil surface to the top of the canopy. Such changes are implicitly included in the turbulent transfer and radiation routines in the model. Therefore, evapotranspiration dynamics controlled by different canopy characteristics were well-represented in our modeling approach (see 2.6 for more detail).

We used a semi-distributed simulation approach by implementing the SHAW model for 21 HRUs for UBB, which were defined based on aspect, elevation, slope, and harvest history. Eight HRUs were first delineated (Wei et al., 2016) based on similar vegetation in 2002 as well as prevailing aspect (S = south, W = west, N = north) and elevation (L = low, M = mid, H = high) (Fig. 1, Table S1). Distinct climate drivers were used for each of these eight original HRUs to account for spatial variations in microclimate based on a network of 18 meteorological stations (see online supplementary material and Wei et al, 2016 for more details). We then further partitioned 13 additional HRUs from these eight HRUs to delimited discrete harvest events; i.e., each new HRU represented the area associated with one harvest event (Table S2; Fig. 1d; e.g., "1966" indicates the HRU that was logged in 1966), which makes it possible to simulate vegetation dynamics in the harvested areas. These new HRUs used identical climatic drivers to the original HRU from which most of their area was partitioned.

The SHAW model was calibrated and validated with observed data for UBB in Wei et al. (2016) for the water years 2004–2009. The model was minimally parameterized (Kirchner, 2006) to retain the chance that the model will fail to reasonably represent observations if it does not accurately represent key physical processes or was unreasonably parameterized. To avoid issues of parameter uncertainty and equifinality that could substantially alter our conclusions, we used a multi-objective parameterization approach that calibrated individual parameters against relevant model outputs (Wei et al., 2016). Following Efstratiadis and Koutsoyiannis (2010), we note that multi-objective calibrations against not only multiple sites or responses (such as high and low flows), but also against multiple hydrologic variables (such as snow water equivalent and transpiration), can reduce equifinality and attendant uncertainty as have been noted in other modeling investigations (Kuppel et al., 2018; Széles et al., 2020). Specifically, snow depth and water equivalent were used to calibrate the rain-snow temperature threshold. Sap flow-based transpiration estimates were used to estimate minimum stomatal resistance and the responsiveness of stomatal resistance to environmental conditions. Soil moisture observations were used to refine estimates of soil hydraulic parameters. Following these calibration efforts, the model reasonably simulated interannual streamflows.

We estimated the model efficiency in this study in terms of Nash-Sutcliffe model efficiency (NSE, Nash and Sutcliffe, 1970) and the relative performance measure ($R_{relative}$) (Seibert et al., 2018). NSE is calculated as follows:

$$NSE = 1 - \left(\frac{\sum_{i=1}^{n} (x_{obs} - x_{sim})^2}{\sum_{i=1}^{n} (x_{obs} - x_{ave})^2} \right) \tag{2}$$

where x_{sim}, x_{obs}, and x_{ave} are simulated values, observed values, and mean of observed values respectively; n is number of pairs of compared values. NSE values indicated model efficiency which ranged from -∞ to 1, where NSE = 0 indicates that the model predicts as accurately as the observed mean, NSE = 1 indicates a perfect match between simulations and observations, and NSE < 0 indicates a worse model performance than the mean.

We also applied the relative performance measure ($R_{relative}$) to estimate the efficiency of a simulation relative to a suite of simulations with possible parameter sets and selected the best model parameter (Seibert et al., 2018) as:

$$R_{relative} = \frac{R_x - R_{lower}}{R_{upper} - R_{lower}} \tag{3}$$

where the upper benchmark (R_{upper}) is suggested to be the best possible simulation that a model can achieve; and the lower benchmark (R_{lower}) to be the minimum expectation of a model with fundamental hydrological processes (see more details in Seibert et al., 2018). We applied

the $R_{relative}$ measure to this study to select the vegetation parameter and scenario that best represented the vegetation dynamics and changes in the water budget. R_{upper} and R_{lower} were determined based on uncertainty analyses of minimum stomatal resistance for each vegetation type, described in detail in the next section.

2.6. Model implementation

We estimated the impact of vegetation changes on streamflow to quantitatively represent how vegetation in the HRUs changed over time. Although the SHAW model reasonably simulated the water budget in UBB in Wei et al. (2016), these simulations only covered the water year 2004 – 2009 and the long-term vegetation changes were not considered. We obtained most parameters from Wei et al. (2016) but three key components differed from this previous study to represent the moderate but important functional long-term changes in vegetation, which were the changes in species composition, small timber harvest experiments, and forest growth. We applied five scenarios to represent these vegetation changes, including: 1) ***NoVeg***, in the absence of vegetation and thus without transpiration; 2) ***ShadeTol***: using the shade-tolerant vegetation throughout the modeled time series with streamflow simulations that were calibrated based on observations from 2000 to 2009; 3) ***WWP***, using the historical white-pine dominated vegetation as model inputs, with streamflow simulations that were calibrated based on observations from 1940 to 1949 prior to blister rust, logging, and climate change throughout the simulated time series (1940–1949); 4) **log**, which estimated the temporal dynamics of logging, recovery, and species replacement in the absence of blister rust over the simulated time series; and 5) **log** + ***rust***, which estimated the temporal dynamics of mortality caused by blister-rust invasion, logging, recovery, and species replacement over the simulated time series that is the most realistic representation of the actual vegetation dynamics within the study watershed.

The first scenario, S_{NoVeg}, used identical parameters to the others except that vegetation biomass, height, and LAI were all set to 0 throughout the simulation period. Thus transpiration was eliminated and any evapotranspiration simulated by the model was driven by abiotic processes. Comparing simulations of other vegetation scenarios with S_{NoVeg} reveals the vegetation effects, especially on evapotranspiration. The S_{WWP} and $S_{ShadeTol}$ scenarios set sideboards on the analysis by assuming constant vegetation as found in either 1940s (western white pine dominated) or 2000s (shade-tolerant species dominated). This approach is similar to those used to assess the hydrological effects of discrete land cover changes following fire (Seibert et al., 2010). Thus, scenarios S_{WWP} and $S_{ShadeTol}$ gave an indication of the species replacement effects in the absence of disturbances and regrowth. Specifically, we applied identical vegetation height (17.6 m), LAI (7.3 m^{-2} m^{-2}), and biomass (31.7 kg m^{-2}) across all 21 HRUs based on LiDAR-estimated unharveted forest (Wei et al., 2016) and vegetation remained unchanged in all years. The minimum stomatal resistance (r_{s0}) was the only parameter that differed between the two scenarios. The r_{s0} value was determined by simulating streamflow with a pool of r_{s0} values from 72 to 422 s m^{-1} with a 10 s m^{-1} increment (Fig. S4); this range of r_{s0} should cover the wide range of variations in r_{s0} from WWP (low r_{s0}) to shade-tolerance tree species (high r_{s0}) in this area (Pangle et al., 2015). The r_{s0} value with the largest $R_{relative}$ in simulating annual streamflow in 1940s was selected for S_{WWP} and that for 2000s was selected for $S_{ShadeTol}$. R_{upper} and R_{lower} were set as the maximum and minimum NSE values among all simulations respectively. While other vegetation parameters may create some uncertainty in historical simulations, r_{s0} and LAI are the vegetation parameters with the greatest impact on hydrologic fluxes in SHAW (Marshall et al., 2021). LAI was relatively well constrained based on basal area records from the permanent plots and 3-PG model simulations (Figs. S2 and S3).

Besides the three constant-vegetation scenarios, we implemented two scenarios to represent the hydrological effects of vegetation dynamics resulting from harvest, blister rust, and regrowth (Fig. 5). The first of these (S_{log}) was set to estimate the effect of sporadic harvests on the water budget, and the second ($S_{log+rust}$) estimated the combined effects of harvest and blister-rust mortality. $S_{log+rust}$ also accounted for the gradual replacement of WWP by shade-tolerant species and was intended to represent the actual historical vegetation changes in UBB. S_{log} began with the same static WWP vegetation as in S_{WWP} and remained unchanged in unlogged HRUs, but all WWP vegetation was removed in each logged HRU in its respective harvest year (Fig. 1d). The shade-tolerant vegetation then emerged in these logged HRUs and the vegetation height, LAI, and biomass were updated every year after logging. As noted above, the growth data after logging were obtained from well calibrated and validated model simulations of similar shade-tolerant forest in an experimental watershed ~130 km south of PREF, which simulated forest regrowth after logging in the 1930s (Du et al., 2016; Wei et al., 2014; Wei et al., 2018) (Fig. S3; see 2.2 for detail). The primary difference between this and the S_{log} simulation was that the static WWP vegetation was gradually replaced due to blister-rust induced mortality (Fig. 5) that most closely matched the forest history in the watershed. The basal areas in Fig. 4 were translated into matching biomass, LAI, and vegetation height (Fig. S3) based on simulated forest growth in Wei et al. (2014) (see 2.2 for detail). The implementation of these scenarios made it possible to estimate the effects of transpiration from the observed vegetation changes ($S_{log+rust}$ – S_{NoVeg}), species replacement alone (S_{WWP} – $S_{ShadeTol}$), harvest alone (S_{log} – S_{WWP}), and blister rust alone (S_{log} – $S_{log+rust}$). We compared the model efficiency across five scenarios with $R_{relative}$. The R_{upper} and R_{lower} were set as the maximum and minimum NSE values among all simulations in five scenarios combined with the simulations with r_{s0} values from 72 to 422 s m^{-1} respectively.

Due to the importance of winter precipitation in the water cycle at the study watershed, we compared the snow simulations with observations to test if snow regimes may have contributed to the changes in the water budget. We ran the model based on the Headquarters site, to test the quality of the simulation of snow depth and SWE. We chose this site as it has snow depth data since 1911 and SWE data since 1936. We

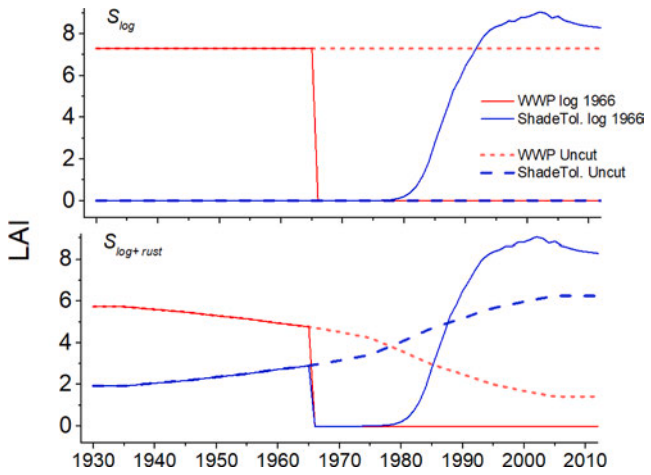

Fig. 5. The schematic figure for vegetation dynamics in terms of changes in LAI in one unharvested and one harvested HRU in two scenarios: S_{log}, WWP vegetation combined with logging events and growth of new shade-tolerant forest after logging; and $S_{log+rust}$, logging combined with changes in vegetation composition shown in Fig. 4, which represented the blister rust-induced WWP mortality and the regeneration and growth of shade-tolerant species. Here we use the 1966 logging HRU as an example. Shade-tolerant species emerged after logging and the vegetation growth data were obtained from 3-PG model simulations (Fig. S3). Other logged HRUs (not shown) were set up similarly to the 1966-HRU: vegetation was the same as in unharvested HRUs before logging, but differed from the unharvested area after logging. Eight unharvested HRUs represent 70% of the area and 13 logged HRUs comprised 30% of the land area in UBB.

applied all but the vegetation parameters from Wei et al. (2016) to the simulation of the Headquarters site as it was located in a small clearing where there was no canopy effect on snow dynamics. Simulations were driven by on-site precipitation and temperature data at Headquarters; wind speed, shortwave radiation, and absolute humidity data were identical to the data for the eight primary HRUs.

3. Results

3.1. Forest composition changes

The 21 permanent monitoring plots with >60 year records revealed the forest composition change at PREF (Fig. 4 and Fig. S2). The mean basal area of WWP began a continuous decline in the 1960s (23.5 m^2 ha^{-1}) that continued until the last observation in the 2000s (6.0 m^2 ha^{-1}) (Fig. 4). We defined the starting point of decreased basal area as the measurement time after which basal area declined in two consecutive measurements. Among 20 plots with decreased WWP basal area, the starting point varied from the 1940s to the 1970s across plots: five plots for the 1940s, four plots for the 1950s, eight plots for the 1960s, and three plots for the 1970s (Fig. S2). Therefore, the 1940s-1970s were noted as the period when blister rust-induced WWP mortality was initiated within different stands in the watershed.

In comparison, the mean basal area of shade-tolerant conifers steadily increased from the 1930s (6.8 m^2 ha^{-1}) to the 2000 s (26.9 m^2 ha^{-1}) at all 21 plots (Fig. S2 and Fig. 4). Consequently, the changes in the mean total basal area (WWP and shade-tolerant conifers) of 21 plots were less dramatic relative to WWP or shade-tolerant conifers from the 1930s to the 2000s and the total basal area was again approaching the 1960s maximum by the 2000s.

3.2. Annual and seasonal changes in hydrometeorology

Annual streamflow increased significantly from 1939 to 2010 at UBB, while annual precipitation, T_{min}, T_{max}, and snow depth did not significantly change based on Mann-Kendall analysis (Table 1). Observed streamflow at UBB increased significantly (based on Sen's slope) for the eight months from late summer through winter (August – March) from 1939 to 2010 (Table 1; Fig. S5); no significant increase occurred in the spring and early summer months (April-July) typically characterized by snowmelt runoff. Meanwhile, precipitation and snow depth did not change significantly in any months, and temperature changes were significant in only three months: T_{min} increased in March and decreased in October, while T_{max} decreased in December at the Headquarters site.

3.3. Hydrologic model performance and calibration results

The SHAW model reasonably simulated snow depth at the Headquarters site (Fig. 6). The Nash-Sutcliffe model efficiency was 0.85 for the days with either observed or simulated snow depth >0 throughout the simulation period.

Based on the $R_{relative}$ values, r_{s0} = 82 s m^{-1} best simulated the streamflow in the 1940s and r_{s0} = 412 s m^{-1} in the 2000s (Fig. 7a). Therefore, we used $r_{s0} = 82$ s m^{-1} for the WWP vegetation and $r_{s0} = 412$ s m^{-1} for the shade-tolerant vegetation.

3.4. Vegetation change scenarios

The static vegetation scenarios, $S_{ShadeTol}$ and S_{WWP}, demonstrated the water budget components in UBB if vegetation stayed unchanged as either of the functional forest types. Simulated annual streamflow averaged 533 and 343 mm (190 mm difference) and likewise ET + ΔS averaged 481 and 671 mm (190 mm difference) for $S_{ShadeTol}$ and S_{WWP} respectively, from water year 1940 to 2009 (Fig. 8b and d). Therefore, the 190 mm difference demonstrated lower annual transpiration and higher streamflow contributions for the shade-tolerant vegetation relative to the WWP vegetation from the 1940s to 2000s.

The simulated vegetation dynamics reasonably explained historical changes in the annual streamflow. The most realistic vegetation scenario $S_{log+rust}$ best simulated the annual streamflow when compared with observations (Fig. 8). This is represented by the best model performance values in terms of NSE (0.30, 0.33, 0.54, 0.63 for $S_{ShadeTol}$, S_{WWP}, S_{log}, and $S_{log+rust}$ respectively) and R^2 between simulations and observations (0.53, 0.52, 0.62, and 0.66, respectively; Fig. S6). $S_{log+rust}$ also best simulated streamflow throughout all years as is shown in the highest $R_{relative}$ of all years among five scenarios, the historical changes in residuals between simulated and observed streamflow (Fig. 8c), and the distributions of data in the scatter plots between simulated and observed streamflow (Fig. S6). Moreover, $S_{log+rust}$ best represented the annual variations for ET + ΔS (Fig. 8d; equivalent to P -Q) and (ET + ΔS)/P (Fig. 8e).

Comparing across scenarios revealed the effects of vegetation changes on the water budget. First, differences in simulations between S_{log} and S_{WWP} demonstrated the changes in water budgets caused by harvests. The difference in annual streamflow and ET between S_{log} and S_{WWP} departed from zero after the first harvest event in 1966 (Fig. 8f and g). The difference in streamflow ranged from 52 to 116 mm and increased with time from water year 1967 to 2009 at a rate of 0.51 mm $year^{-1}$ (linear regression, $p < 0.01$, $R^2 = 0.16$). Second, the difference in ET ranged from −46 to −125 mm and decreased at a rate of 0.55 mm $year^{-1}$ ($P < 0.01$, $R^2 = 0.19$; Fig. 8d). Third, the difference between $S_{log+rust}$ and S_{log} demonstrated the impact of WWP mortality due to blister rust (Fig. 8f and g). Differences in annual streamflow ranged from −1 to 81 mm (0.80 mm $year^{-1}$, $p < 0.01$, $R^2 = 0.70$) and differences in annual ET ranged from 2 to –81 mm (–0.77 mm $year^{-1}$, $p < 0.01$, $R^2 = 0.66$). Fourth, differences between $S_{log+rust}$ and S_{WWP} demonstrated the combined vegetation changes (WWP mortality, logging, and regeneration of shade-tolerant species). Differences in streamflow ranged from −1 to 180 mm (2.50 mm $year^{-1}$, $p < 0.01$, $R^2 = 0.81$; Fig. 8f) and differences in ET from 2 to −221 mm (−2.42 mm $year^{-1}$, $p < 0.01$, $R^2 = 0.80$; Fig. 8g) from water year 1940 to 2009.

The simulations with S_{NoVeg} indicate the expected change in streamflow in an unvegetated scenario (Fig. 9). Despite similar year-to-year variations in streamflow (Fig. 9a), simulated annual streamflow in S_{NoVeg} was higher than $S_{log+rust}$ ($S_{NoVeg} - S_{log+rust}$) and observations (S_{NoVeg} – Obs.) (Fig. 9b) as would be expected for only abiotically-driven evaporative processes. Such differences in streamflow decreased with

Table 1
Trends in annual and monthly streamflow (Q) at UBB and climatic factors, including daily maximum temperature, (T_{max}), daily minimum temperature (T_{min}), precipitation (P), and snow depth ($Snow$) at the Headquarters station from 1939 to 2010 based on Mann-Kendall analysis. Numbers indicate Sen's slopes (mm $year^{-1}$ for streamflow and precipitation; °C $year^{-1}$ for temperatures) and symbols for p values ("*", $0.01 < p \leq 0.05$; "**", $p \leq 0.01$; "–", $p > 0.05$). The "×" symbols in snow depth results indicate that Mann-Kendall analysis was not conducted for these months with >80% zero values.

	Annual	Jan	Feb	Mar	Apr	May	Jun	Jul	Aug	Sep	Oct	Nov	Dec
Q	3.28*	0.16**	0.18*	0.43**	–	–	–	–	0.09**	0.08**	0.07**	0.07**	0.10*
T_{max}	–	–	–	–	–	–	–	–	–	–	–	–	*−0.029***
T_{min}	–	–	–	0.027**	–	–	–	–	–	–	*−0.023**	–	–
P	–	–	–	–	–	–	–	–	–	–	–	–	–
$Snow$	–	–	–	–	–	×	×	×	×	×	×	–	–

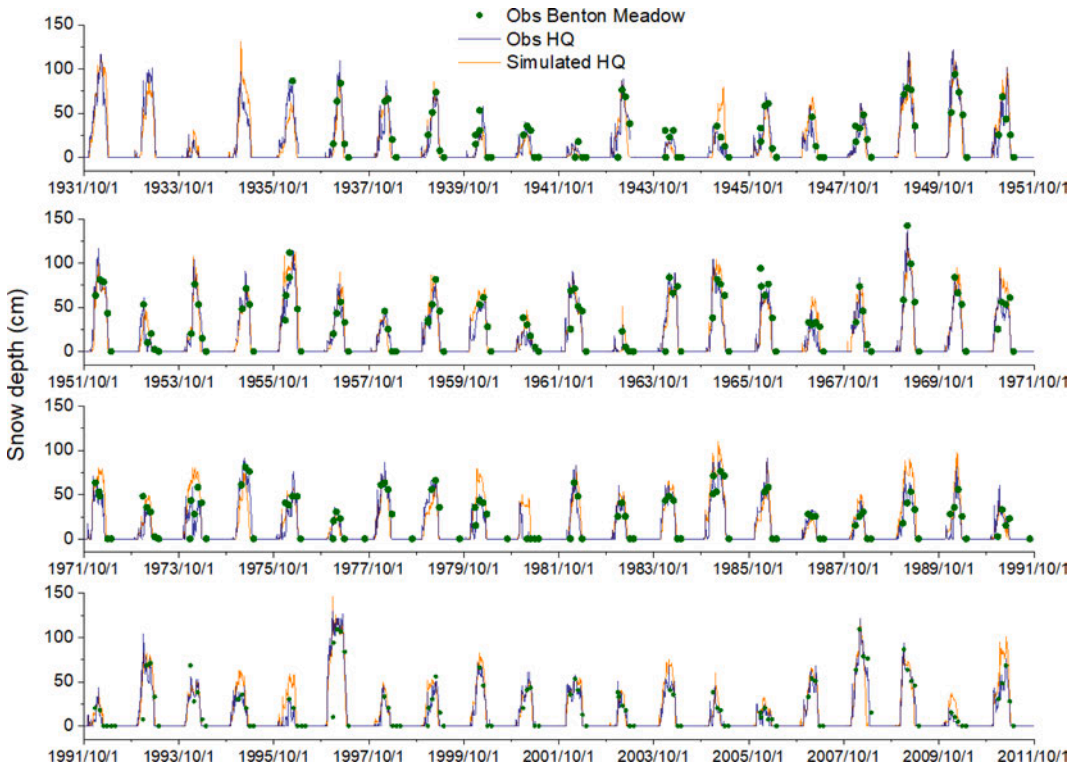

Fig. 6. Simulated and observed snow depth at the Headquarters (HQ) site. The HQ site is located at a lower elevation outside the UBB, where two sets of snow depths were recorded (daily at HQ and monthly at Benton Meadow near HQ).

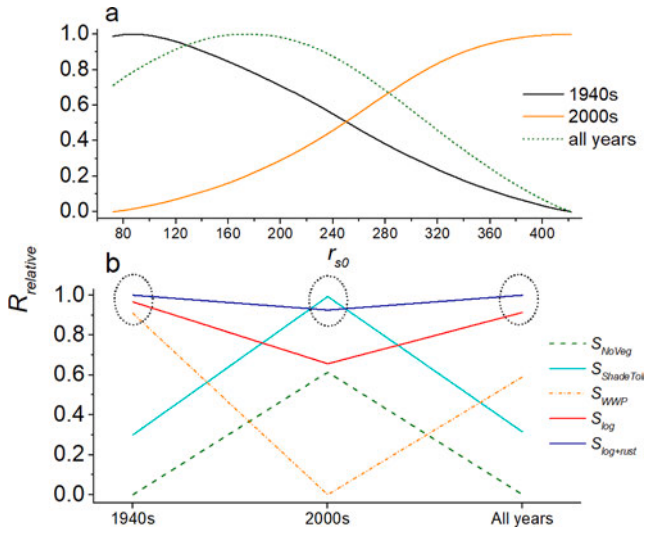

Fig. 7. Relative performance measures ($R_{relative}$) of simulating annual streamflow with (a) varied minimum stomatal resistance (r_{s0}) and (b) different vegetation scenarios in the 1940s, 2000s, and all years from 1940s to 2000s. The r_{s0} values that provided the highest $R_{relative}$ in the 1940s and 2000s were used for simulating WWP vegetation (r_{s0} = 82 s m^{-1}) and shade-tolerant vegetation (r_{s0} = 412 s m^{-1}), respectively. Simulations in (b) were based on five scenarios (S): S_{NoVeg}, no vegetation; $S_{ShadeTol}$, shade-tolerant vegetation in the 2000s (representing mixed fir-hemlock-cedar forests, no growth); S_{WWP}, historical WWP–dominated vegetation in 1940s (no growth); and S_{log} and $S_{log+rust}$ (see the caption in Fig. 5). $S_{log+rust}$ best simulated the annual streamflow of all years.

time (linear regression; R^2 = 0.32 and 0.41, and slope = −2.91 and −2.19 mm year^{-1} for S_{NoVeg} – Obs and S_{NoVeg} – $S_{log+rust}$ respectively, both $p < 0.01$), which reflects decreases in transpiration through the simulation years in $S_{log+rust}$ (Fig. 9b). These differences illustrate the magnitude of historical decreases in transpiration. This also indicates the potential immediate increases of streamflow if mortality occurred over the entire watershed, which ranged from roughly 500 mm to 300 mm depending on the vegetation type.

We summarized the evidence for causes of historical changes in streamflow in Fig. 10, which indicated a ~128–179 mm increase between the 1940s and the 2000s. We used S_{NoVeg} and S_{WWP} as sideboards; these two scenarios assumed zero (S_{NoVeg}) or limited (S_{WWP}; only responded to climate changes) changes in transpiration due to vegetation changes. $S_{ShadeTol} - S_{WWP}$ indicates how the shade-tolerant and WWP vegetation may respond differently to the climate in each decade assuming static vegetation; their difference should also reflect the impact of vegetation changes on streamflow in the 2000s. Therefore, the relative changes between simulated streamflow of S_{NoVeg}/S_{WWP} and $S_{log+rust}$ indicate changes in streamflow due to changes in vegetation (differences were normalized with 1940s' difference = 0 mm). The changes in streamflow increased with time (R^2 = 0.92 and 0.91, and slope = 3.2 and 2.5 mm year^{-1} for $S_{log+rust} - S_{NoVeg}$ and $S_{WWP} - S_{NoVeg}$, respectively; both $p < 0.01$). The mean annual difference was 179 mm for $S_{log+rust} - S_{NoVeg}$ and 128 mm for $S_{log+rust} - S_{WWP}$ in the 2000s. Moreover, we compared simulated streamflow between two static vegetation scenarios ($S_{ShadeTol} - S_{WWP}$), which assumed that vegetation did not change through time. The difference was 153 mm in the 2000s, similar to $S_{log+rust} - S_{NoVeg}$ and $S_{WWP} - S_{NoVeg}$.

4. Discussion

This study revealed historical changes in the water budget in a small watershed in the U.S. interior Pacific Northwest that were mainly caused by the mortality of WWP and small-scale forest harvests. We simulated the water budget at UBB based on minimally tuned parameters to represent the change in forest composition. Changes in water budget and increases in streamflow can be explained by the simulated vegetation changes, including the impacts of WWP mortality, timber harvesting,

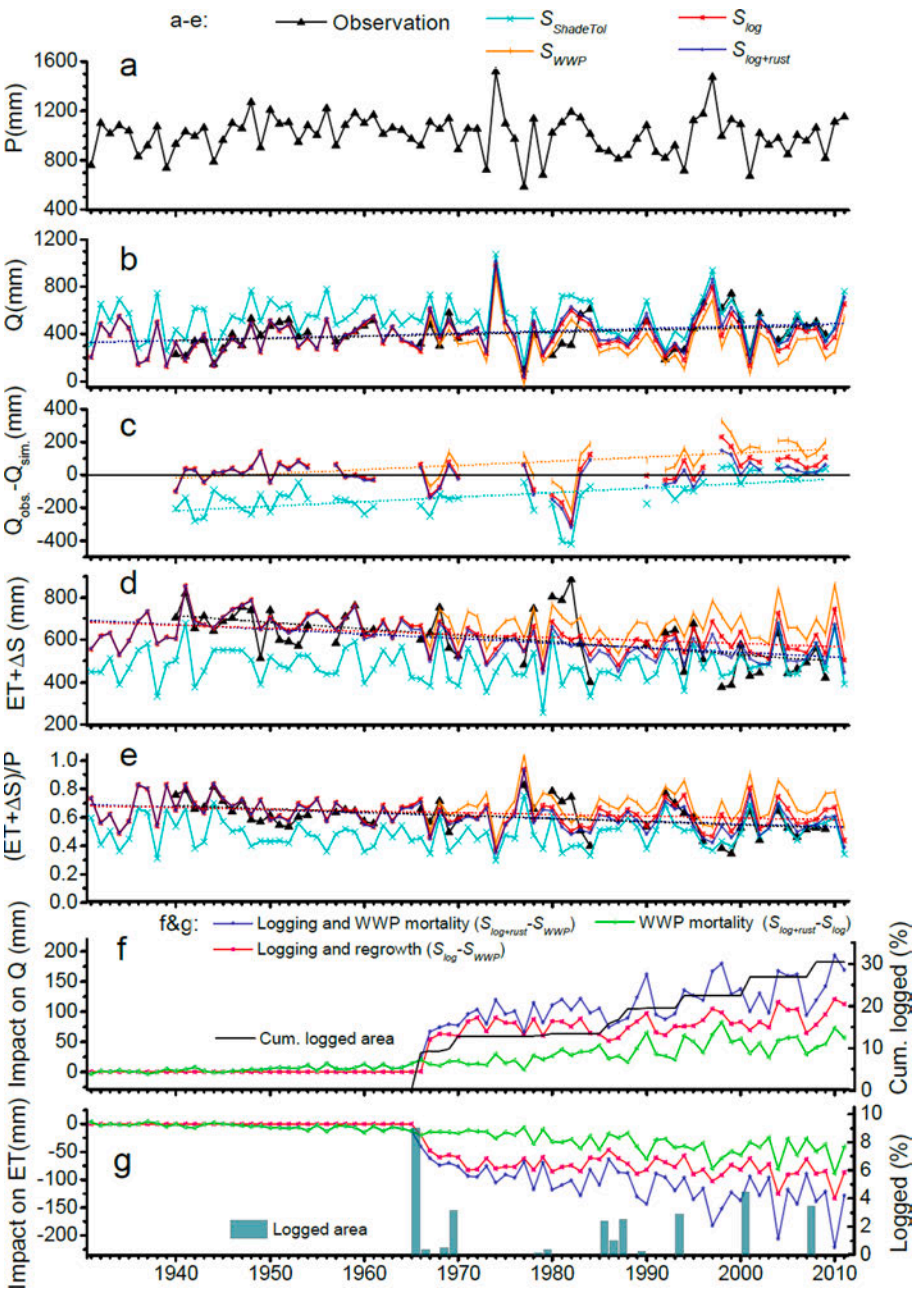

Fig. 8. Observed and simulated water budgets in UBB. (a) Observed precipitation (*P*). (b) Observed and simulated streamflow (*Q*). (c) The residual between simulated and observed streamflow decreased significantly with time in $S_{ShadeTol}$ and S_{WWP} but not in other scenarios; $S_{log+rust}$ best simulated the changes in annual streamflow among all scenarios with the lowest residual. (d) Simulated ET + ΔS and observed P-Q (equivalent to ET + ΔS based on Eq. (1)). (e) Simulated (ET + ΔS)/P and observed (P-Q)/P. Estimated impacts of logging + regrowth and WWP mortality on annual streamflow (f) and ET (g). Cumulative logged area (%) and logged area in a single year (%) are shown in Fig. f and g, respectively. Compared with the simulations with four scenarios, changes in observed streamflow and ET were best explained by $S_{log+rust}$ in terms of the lowest residuals between simulations and observations and the closest slopes in linear regressions. Dotted lines in Fig. b-e indicate significant linear regressions ($P < 0.05$) for visual estimation of trends; the horizontal line in Fig. c indicates residual = 0. All regression tests were conducted from water year 1940 to 2009 (i.e., the period with observed streamflow).

and regrowth by representing the observed vegetation dynamics (Fig. 8). Simulation of the most realistic vegetation scenario ($S_{log+rust}$) closely represented historical changes in observed streamflows from the 1940s to the 2000s (Fig. 8 & Fig. 9); this scenario should also provide insights into the water budget when observed streamflow was incomplete, especially in the 1960–1980s.

4.1. Causes for streamflow changes

A key question is how much has streamflow increased, and why? Combining multiple lines of evidence provided a new quantitative understanding of this question (Figs. 8-10). First, the trends in temperature, precipitation, and snow depth cannot explain increases in annual and monthly streamflow from August to March. Warming annual temperatures (Fig. 2) should result in reduced streamflows rather than increases due to increasing evaporative demand and differences in snow vs. rain-driven hydrology (Berghuijs et al., 2014; Liu et al., 2022). Long-term temperature increases were only significant for the annual minimums and were very subtle, in contrast to more pronounced regional trends (Dalton et al., 2013) possibly because cold-air drainage contributed to inversions at the site (Duursma pers. comm.) that led to local atmospheric decoupling as has been observed at other mountainous sites in the region (Daly et al., 2010; Wei et al., 2018). Observed annual precipitation in PREF did not change significantly at the PREF headquarters (726 m a.s.l) (Table 1 and Fig. 2), though there was no high-elevation precipitation observation at the highest elevation in PREF (1700 m), which is generally lower than other mountain ranges in the broader region over which widespread declines have been noted (Luce et al., 2013). Seasonally, an increase in T_{min} in March may explain an increase in streamflow in this month potentially due to increases in snowmelt. Cooler temperatures in October and December should reduce evapotranspiration and may hence increase streamflow, but temperature and precipitation do not explain streamflow changes in other months. Therefore, it is likely that the increases in monthly streamflow

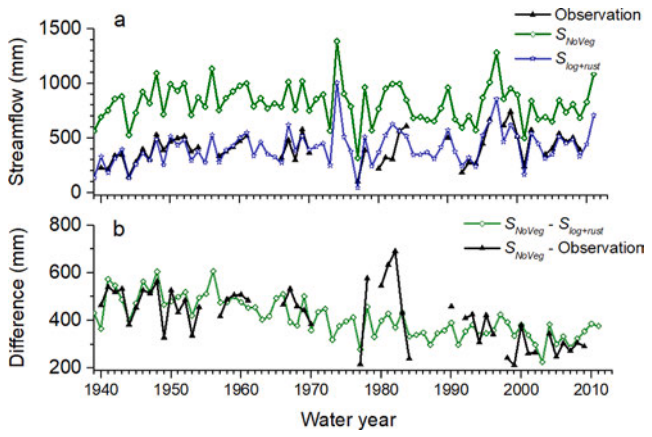

Fig. 9. Simulated streamflow without vegetation. (a) Observed annual streamflow and streamflow simulations without vegetation (S_{NoVeg}) and with observed vegetation ($S_{log+rust}$). (b) Differences between streamflow simulations between S_{NoVeg} and $S_{log+rust}$, and between S_{NoVeg} and observation.

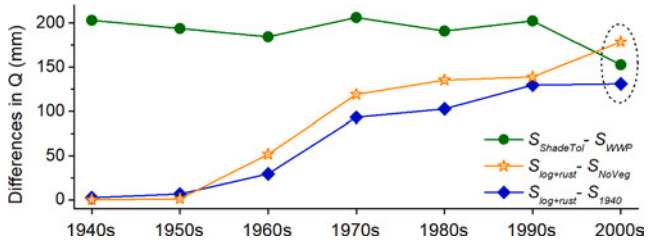

Fig. 10. Decadal summary of changes in simulated streamflow in UBB, showing differences in decadal-average Q between $S_{ShadeTol}$ and S_{WWP} (green); $S_{log+rust}$ and S_{NoVeg} (orange); and $S_{log+rust}$ *and* S_{WWP} (blue). Circled data points highlight the estimated differences in streamflow due to vegetation change scenarios. (For interpretation of the references to colour in this figure legend, the reader is referred to the web version of this article.)

were caused by vegetation changes that reduced evapotranspiration and hence increased streamflow in these months.

Hydrological simulations provided more evidence about how vegetation changes have likely increased streamflows. As the second line of evidence, the lack of a trend in simulated streamflow in the fixed-vegetation scenarios ($S_{ShadeTol}$, S_{WWP}, and S_{NoVeg}; Fig. 8b & Fig. 9a) indicates that changes in climate were not responsible for the observed streamflow increases. The difference between simulations with shade-tolerant ($S_{ShadeTol}$) and WWP vegetation (S_{WWP}) demonstrated how streamflow would change if vegetation stayed unchanged. $S_{ShadeTol}$ produced 153 mm higher streamflow than S_{WWP} in the 2000s (Fig. 10). Third, simulated streamflow increased gradually with the more realistic vegetation dynamics ($S_{log+rust} - S_{WWP}$) from the 1940s to the 2000s, and the difference was 131 mm in the 2000s (Fig. 10). Fourth, when we use the simulation without vegetation (S_{NoVeg}) as a reference (Fig. 9b), the normalized difference increased with time and reached 179 mm by the 2000s. Therefore, we estimated that there was approximately 131–179 mm of increase in streamflow from the 1940s to the 2000s based on the three lines of evidence (2nd-4th) above. This indicated that ~30–40% of the observed streamflow (443 mm in the 2000s; Fig. 8f) by the 2000s could be attributed to blister rust-related WWP mortality with subsequent replacement by shade-tolerant species.

We hypothesized that WWP mortality and timber harvest should increase streamflow, and such change could be pronounced since WWP transpires approximately twice as much water relative to regenerated shade-tolerant species, based on a study in PREF that utilized sap flow measurements (Pangle et al., 2015). One may expect that WWP mortality should have played a larger role in the increased streamflow than timber harvests, as cumulatively only ~30% of the area was harvested in 13 separate years from 1966 to 2008 (mean of 2.3% per entry), and that the impacts of small harvests on streamflow would be minor (Stednick, 1996). However, the impact of WWP mortality on streamflow increased slowly since the 1940s and reached 44 mm per year (~1/3 of the total change) by the 2000s based on the hydrological simulations; in contrast, the impact of limited harvest, regeneration, and growth of shade-tolerant species started after the first logging event in 1966 during the simulation period and reached 87 mm (~2/3 of the total change) by the 2000s (Fig. 8f). Therefore harvest actually produced about twice as much change in streamflow relative to WWP mortality by the 2000s. Such continuous impact of harvest may be related to a combination of much larger flow changes following harvest and the slow hydrological recovery after harvest in this region which could take approximately 50 years based on a similar modeling study in the region (Du et al., 2016).

This study provides distinctive information about the combined effect of species composition changes and forest harvest, making it difficult to compare quantitatively with other studies. However, if we only compare the effect of timber harvest, a 27 km^2 watershed in northern Idaho (Mica Creek Experimental Watershed; MCEW) ~130 km away from UBB may serve as the closest comparison with a similar elevation (MCEW 945–1650 m; UBB 805–1700 m) and vegetation. MCEW is currently covered with shade-tolerant species which regenerated from the clearcut around the 1930s (Wei et al., 2018). A paired and nested watershed study with seven sub-watersheds was conducted in 1997 for road construction (2–3% watershed area) and in 2001 for timber harvest at MCEW (Du et al., 2014; Du et al., 2016; Srivastava et al., 2020). In addition to small hydrological impacts from road construction, increases in annual streamflow were observed as a function of the clearcut area: 284 mm (34% increase) from 50% clearcut vegetation removal and 161 mm (23% increase) from 25% partial-cut vegetation removal based on 16-years of data from 1992 to 2007 (Srivastava et al., 2020). In comparison, UBB experienced a ~87 mm (~20% increase) in streamflow between the 1940s and 2000s due to a cumulative 30.4% harvested area. Such an increase in streamflow per harvested area was lower than MCEW as well as the mean water yield increment across 29 watersheds with partial-cut, thinning, or strip cut across the globe (145 mm increase) (Picchio et al., 2021). The smaller changes per harvested area at UBB likely resulted from the prolonged harvest period at UBB (13 events from 1966 to 2008), which would reduce cumulative impacts on streamflow due to ample time for forest recovery.

Another vegetation factor that may have played a role in water budget alterations is native root diseases, although their impact is not clear at this stage. Native root diseases occurred on the shade-tolerant conifers and reduced tree vigor and transpiration (Cruickshank et al., 2011; Neuenschwander, et al., 1999). It was difficult to separate such an impact on transpiration at the watershed scale as the mortality of WWP and harvest also contributed to transpiration changes. Moreover, the basal area of shade-tolerant conifers increased continuously in PREF since the 1930s (Fig. 4); such active growth would increase evapotranspiration (both canopy interception and transpiration) and hence potentially conceal the lesser impact of root diseases on the water budget. We lacked a detailed record on the root diseases and a quantitative estimate of their ecophysiological impact in this area. Therefore, further studies are necessary to reveal the additional nuance of root diseases on historical changes in the water budget.

4.2. *Assumptions and limitations*

This study highlighted the importance of long-term forest ecohydrological observations. Despite the large scale of WWP mortality and the shift to more shade-tolerant species, it is difficult to quantify the hydrological impact of such an event that occurred gradually over decades and concomitantly with changes in other vegetation parameters that affect hydrological partitioning. The long-term data made it possible to retrospectively compare differences in the water budget from

hydrometeorology (since 1910s), streamflow (since 1930s), and vegetation records (since 1910s) at PREF. These data made it possible to reveal the mechanisms responsible for apparently anomalous changes in the water budget since the 1930s due to vegetation changes, most notably the shift in species composition and harvest events.

This study should be informative to estimate hydrological changes in surrounding areas with historical WWP mortality. In northern Idaho, intensive logging occurred in the late 19th century (Neuenschwander, et al., 1999; Strong and Webb, 1970) and an extensive high severity fire occurred in (the "Big Burn") in 1910 (Fig. S1) (Diaz and Swetnam, 2013; Egan, 2009; Plummer, 1912). The impact of vegetation changes on the water budget should be more dramatic in these affected areas than in UBB. However, two major factors limit thorough analyses of hydrological dynamics in most locations. First, streamflow data are not available because most hydrological stations were established after the disappearance of WWP. For example, extensive forest clearing was reported in the Priest River, Shoshone, and the Clearwater River regions in the early 20th century (Strong and Webb, 1970), and the "Big Burn of 1910" consumed much of the forested area in northern Idaho (Fig. S1). Therefore, very limited areas were left where hydrometeorological data were available for tracking the period of WWP mortality and subsequent regeneration (Fig. S1). Second, although the reduced transpiration should increase water available for streamflow, such increasing streamflow trends are counter to the regional trend of declining streamflows likely caused by climate change (Wei et al., 2016). A prevailing regional trend of decreasing observed streamflows from 1950 to 2006 in basins across the broader region (Luce and Holden, 2009), appears to be due to the reduced strength of westerlies in the Pacific Northwest leading to decreasing orographic precipitation at high elevations and, to a lesser degree, rising temperature and evapotranspiration (Luce et al., 2013). Therefore, the possible increase of streamflow due to WWP mortality in the montane regions may have been constrained by a background of decreasing precipitation, warming temperatures, and landcover diversity produced by complex patterns of timber harvest and regeneration in larger watersheds throughout the 20th century. Without these counteracting widespread changes, the impact of WWP mortality could be even larger. Therefore, further studies are required to disentangle the impacts of even more factors than this study on historical changes in the water budget in northern Idaho.

In this study, we simulated historical water budget conditions using an intensively monitored site. Nonetheless, hydrologic simulations of this long period necessarily constitute some uncertainties. Most notably, there is some uncertainty in the historical model parameterization. For instance, a possible risk is that observational uncertainties related to deep percolation or estimation of vegetation characteristics (LAI, height, and biomass) were compensated for by errors in the $r_{s,0}$ calibration. Future work could include a full sensitivity and uncertainty analysis (e.g. Pappenberger and Beven, 2006; Seibert and McDonnell, 2010) in order to address this limitation.

4.3. Management implications

Management implications of this work should be carefully considered. Due to the higher transpiration rates of WWP than currently dominant shade-tolerant species, a naïve interpretation may suggest that WWP restoration should be discouraged to promote higher streamflows in the future with a warmer climate and higher anthropogenic water demand. Our study indicated a limited impact of WWP mortality on streamflow from the 1940s to the 2000s which increased streamflow by ~44 mm by the 2000s. Besides water yield, forest management should also account for multiple values and ecosystem functions across watersheds with diverse landcover; WWP, the tree named "king of many waters" (Strong and Webb, 1970), provided valuable ecological, aesthetic, and economic values for the region (Fins et al., 2002; Harvey et al., 2008). Therefore, we caution that the restoration of WWP ecosystems should consider all the benefits of diverse ecosystem functions that may outweigh potential hydrological detriments of regenerating WWP forests.

5. Summary and conclusions

This study estimated the changes in forest composition and water budget in a small watershed where previously dominant WWP was gradually replaced by shade-tolerant conifers. The 4.0 km^2 UBB provided a data-rich setting to assess the long-term effect of WWP mortality on the water budget, with which we could explore interacting ecohydrological influences on the water budget. We used hydrological simulations to estimate the water budget components under WWP versus shade-tolerant species. Shade-tolerant vegetation in the 2000s transpired less than WWP vegetation in the 1940s, which caused a ~131–179 mm streamflow increase from the 1940s to the 2000s. WWP mortality appeared to result in gradually increasing streamflows since the 1950s, while 13 small-scale harvest events beginning in 1966 further increased streamflow. As a result, WWP mortality increased streamflow by 44 mm (~1/3 of the change), and logging increased streamflow by 87 mm (~2/3) from the 1940s to the 2000s. We assert that similar processes have likely occurred across the region of historic WWP decline, but have been largely unrecognized at larger scales due to other interacting processes including changes resulting from climate trends and variations, land use, and land cover dynamics that have obscured the more subtle species changes. This study highlighted the importance of combining long-term hydrological and vegetational observations and hydrological modeling, to reveal changes in the water budget at the small watershed scale driven by vegetation changes, thereby improving the predictability of streamflow responses to forest disturbance.

Declaration of Competing Interest

The authors declare that they have no known competing financial interests or personal relationships that could have appeared to influence the work reported in this paper.

Acknowledgments

This study is supported by National Science Foundation of China (No. 41991254 and 31971492), United States Forest Service (USFS) Western Wildlands Environmental Threat Assessment Center (WWETAC), and the Rocky Mountain Research Station (RMRS) climate change initiative. John Marshall was supported the Knut and Alice Wallenberg Foundation (#2015.0047), Sweden. We thank Gerald Flerchinger for assistance with the SHAW model, and multiple data providers: Paul Gessler, Andrew Robinson, Aaron Smith, Remko Duursma, Amy Pocewicz, and Robert Pangle.

Appendix A. Supplementary data

Supplementary data to this article can be found online at https://doi.org/10.1016/j.jhydrol.2022.128230.

References

Andréassian, V., 2004. Waters and forests: from historical controversy to scientific debate. Journal of Hydrology 291 (1), 1–27.
Berghuijs, W.R., Woods, R.A., Hrachowitz, M., 2014. A precipitation shift from snow towards rain leads to a decrease in streamflow. Nature Climate Change 4 (7), 583–586.
Berryman, E.M., Marshall, J.D., Kavanagh, K., 2014. Decoupling litter respiration from whole-soil respiration along an elevation gradient in a Rocky Mountain mixed-conifer forest. Canadian Journal of Forest Research 44 (5), 432–440.
Bladon, K.D., Bywater-Reyes, S., LeBoldus, J.M., Keriö, S., Segura, C., Ritóková, G., Shaw, D.C., 2019. Increased streamflow in catchments affected by a forest disease epidemic. Sci Total Environ 691, 112–123.
Brown, A.E., Zhang, L., McMahon, T.A., Western, A.W., Vertessy, R.A., 2005. A review of paired catchment studies for determining changes in water yield resulting from alterations in vegetation. Journal of Hydrology 310 (1), 28–61.

Buttle, J.M., 2011. The Effects of Forest Harvesting on Forest Hydrology and Biogeochemistry. In: Levia, D.F., Carlyle-Moses, D., Tanaka, T. (Eds.), Forest Hydrology and Biogeochemistry: Synthesis of Past Research and Future Directions. Springer, Netherlands, Dordrecht, pp. 659–677.
Chauvin, G.M., Flerchinger, G.N., Link, T.E., Marks, D., Winstral, A.H., Seyfried, M.S., 2011. Long-term water balance and conceptual model of a semi-arid mountainous catchment. Journal of Hydrology 400 (1-2), 133–143.
Cline, R.G., Campbell, G.S. and Haupt, H.F. 1977. Potential Water Yeld Response Following Clearcut Harvesting on North and South Slopes in Northern Idaho.
Coble, A.A., Barnard, H., Du, E., Johnson, S., Jones, J., Keppeler, E., Kwon, H., Link, T.E., Penaluna, B.E., Reiter, M., River, M., Puettmann, K., Wagenbrenner, J., 2020. Long-term hydrological response to forest harvest during seasonal low flow: Potential implications for current forest practices. Sci Total Environ 730, 138926.
Cruickshank, M.G., Morrison, D.J., Lalumière, A., 2011. Site, plot, and individual tree yield reduction of interior Douglas-fir associated with non-lethal infection by Armillaria root disease in southern British Columbia. Forest Ecology and Management 261 (2), 297–307.
Dalton, M.M., Mote, P.W., Snover, A.K., 2013. Climate Change in the Northwest: Implications for Our Landscapes, Waters, and Communities. Island Press, Washington, DC.
Daly, C., Conklin, D.R., Unsworth, M.H., 2010. Local atmospheric decoupling in complex topography alters climate change impacts. International Journal of Climatology 30 (12), 1857–1864.
Diaz, H.F., Swetnam, T.W., 2013. The Wildfires of 1910: Climatology of an Extreme Early Twentieth-Century Event and Comparison with More Recent Extremes. Bulletin of the American Meteorological Society 94 (9), 1361–1370.
Du, E., Link, T.E., Gravelle, J.A., Hubbart, J.A., 2014. Validation and sensitivity test of the distributed hydrology soil-vegetation model (DHSVM) in a forested mountain watershed. Hydrological Processes 28 (26), 6196–6210.
Du, E., Link, T.E., Wei, L., Marshall, J.D., 2016. Evaluating hydrologic effects of spatial and temporal patterns of forest canopy change using numerical modelling. Hydrological Processes 30 (2), 217–231.
Duursma, R.A., Marshall, J.D., Robinson, A.P., 2003. Leaf area index inferred from solar beam transmission in mixed conifer forests on complex terrain. Agricultural and Forest Meteorology 118 (3–4), 221–236.
Efstratiadis, A., Koutsoyiannis, D., 2010. One decade of multi-objective calibration approaches in hydrological modelling: a review. Hydrological Sciences Journal 55 (1), 58–78.
Egan, T., 2009. The Big Burn: Teddy Roosevelt and the Fire That Saved America. Houghton Mifflin Harcourt Publishing, New York.
Fins, L., et al., 2002. Return of the giants: restoring western white pine to the Inland Northwest. Journal of Forestry 100 (4), 20–26.
Flerchinger, G., Cullum, R., Hanson, C., Saxton, K., 1990. Soil freezing and thawing simulation with the SHAW model. Frozen Soil Impacts on Agricultural, Range, and Forest Lands 77–86.
Flerchinger, G.N., Cooley, K.R., Hanson, C.L., Seyfried, M.S., 1998. A uniform versus an aggregated water balance of a semi-arid watershed. Hydrological Processes 12 (2), 331–342.
Flerchinger, G.N., Hanson, C.L., Wight, J.R., 1996. Modeling Evapotranspiration and Surface Energy Budgets Across a Watershed. Water Resources Research 32 (8), 2539–2548.
Goeking, S.A., Tarboton, D.G., 2020. Forests and Water Yield: A Synthesis of Disturbance Effects on Streamflow and Snowpack in Western Coniferous Forests. Journal of Forestry 118 (2), 172–192.
Harvey, A.E., Byler, J.W., McDonald, G.I., Neuenschwander, L.F. and Tonn, J.R. 2008. Death of an ecosystem: perspectives on western white pine ecosystems of North America at the end of the twentieth century.
Jain, T.B. and Graham, R.T. 2005. Restoring dry and moist forests of the inland northwestern U.S, 463-480 pp.
Kirchner, J.W., 2006. Getting the right answers for the right reasons: Linking measurements, analyses, and models to advance the science of hydrology. Water Resources Research 42 (3), W03S04.
Kuppel, S., Tetzlaff, D., Maneta, M.P., Soulsby, C., 2018. What can we learn from multi-data calibration of a process-based ecohydrological model? Environmental Modelling & Software 101, 301–316.
Landsberg, J.J., Waring, R.H., 1997. A generalised model of forest productivity using simplified concepts of radiation-use efficiency, carbon balance and partitioning. Forest Ecology and Management 95 (3), 209–228.
Link, T.E., Flerchinger, G.N., Unsworth, M., Marks, D., 2004. Simulation of Water and Energy Fluxes in an Old-Growth Seasonal Temperate Rain Forest Using the Simultaneous Heat and Water (SHAW) Model. Journal of Hydrometeorology 5 (3).
Link, T.E., Wei, L. and Denner, R.J., 2015. Streamflow data for the Priest River Experimental Forest. Fort Collins, CO: Forest Service Research Data Archive. DOI: https://doi.org/10.2737/RDS-2015-0006.
Liu, Z., Wang, T., Han, J., Yang, W., Yang, H., 2022. Decreases in Mean Annual Streamflow and Interannual Streamflow Variability Across Snow-Affected Catchments Under a Warming Climate. Geophysical Research Letters 49 (3).
Lockman, I.B., et al., 2016. Forest root diseases across the United States. U.S, Department of Agriculture, Forest Service, Rocky Mountain Research Station, Ogden, UT.
Luce, C.H., Abatzoglou, J.T., Holden, Z.A., 2013. The Missing Mountain Water: Slower Westerlies Decrease Orographic Enhancement in the Pacific Northwest USA. Science 342 (6164), 1360–1364.
Luce, C.H., Holden, Z.A., 2009. Declining annual streamflow distributions in the Pacific Northwest United States, 1948–2006. Geophysical Research Letters 36 (16), L16401.
Marshall, A.M., Link, T.E., Flerchinger, G.N., Lucash, M.S., 2021. Importance of Parameter and Climate Data Uncertainty for Future Changes in Boreal Hydrology. Water Resources Research 57 (8).
McDonnell, J.J., et al., 2018. Water sustainability and watershed storage. Nature Sustainability 1 (8), 378–379.
Nash, J.E., Sutcliffe, J.V., 1970. River flow forecasting through conceptual models part I — A discussion of principles. Journal of Hydrology 10 (3), 282–290.
Neuenschwander, L.F. et al., 1999. White pine in the American West: A vanishing species-can we save it?.
Niinemets, Ü., Valladares, F., 2006. Tolerance to shade, drought, and waterlogging of temperate Northern Hemisphere trees and shrubs. Ecological Monographs 76 (4), 521–547.
Pangle, R., Kavanagh, K., Duursma, R., 2015. Decline in canopy gas exchange with increasing tree height, atmospheric evaporative demand, and seasonal drought in co-occurring inland Pacific Northwest conifer species. Canadian Journal of Forest Research 45 (8), 1086–1101.
Pappenberger, F., Beven, K.J., 2006. Ignorance is bliss: Or seven reasons not to use uncertainty analysis. Water Resources Research 42 (5).
Picchio, R., Jourgholami, M., Zenner, E.K., 2021. Effects of Forest Harvesting on Water and Sediment Yields: a Review Toward Better Mitigation and Rehabilitation Strategies. Curr Forestry Rep 7 (4), 214–229.
Plummer, F.G., 1912. Forest fires: their causes, extent, and effects, with a summary of recorded destruction and loss, 117. US Dept. of Agriculture, Forest Service.
Schnepf, C.C. and Schwandt, J.W., 2006. Pruning Western White Pine: A Vital Tool for Species Restoration. PNW 584, A Pacific Northwest Extension Publication. University of Idaho, Oregon State University, and Washington State University.
Seibert, J., McDonnell, J.J., 2010. Land-cover impacts on streamflow: a change-detection modelling approach that incorporates parameter uncertainty. Hydrological Sciences Journal 55 (3), 316–332.
Seibert, J., McDonnell, J.J., Woodsmith, R.D., 2010. Effects of wildfire on catchment runoff response: a modelling approach to detect changes in snow-dominated forested catchments. Hydrology Research 41 (5), 378–390.
Seibert, J., Vis, M.J.P., Lewis, E., van Meerveld, H.J., 2018. Upper and lower benchmarks in hydrological modelling. Hydrological processes 32 (8), 1120–1125.
Slinski, K.M., Hogue, T.S., Porter, A.T., McCray, J.E., 2016. Recent bark beetle outbreaks have little impact on streamflow in the Western United States. Environmental Research Letters 11 (7), 074010.
Srivastava, A., et al., 2020. Modeling forest management effects on water and sediment yield from nested, paired watersheds in the interior Pacific Northwest. USA using WEPP. Sci Total Environ 701, 134877.
Stage, A.R., 1957. Some runoff characteristics of a small forested watershed in northern Idaho. Northwest Science 31 (1), 14–27.
Stednick, J.D., 1996. Monitoring the effects of timber harvest on annual water yield. Journal of Hydrology 176 (1), 79–95.
Strong, C.C., Webb, C.S., 1970. White pine: king of many waters. Mountain Press Pub, Co.
Swank, W.T., Douglass, J.E., 1974. Streamflow Greatly Reduced by Converting Deciduous Hardwood Stands to Pine. Science 185 (4154), 857–859.
Swank, W.T., Miner, N.H., 1968. Conversion of Hardwood-Covered Watersheds to White Pine Reduces Water Yield. Water Resources Research 4 (5), 947–954.
Széles, B. et al., 2020. The Added Value of Different Data Types for Calibrating and Testing a Hydrologic Model in a Small Catchment. Water Resources Research, 56 (10): e2019WR026153.
Teuling, A.J., Hoek van Dijke, A.J., 2020. Forest age and water yield. Nature 578 (7794), E16. E18.
Tinkham, W.T., Denner, R. and Graham, R.T., 2015. Climate, Snowpack, and Streamflow of Priest River Experimental Forest Revisited. Gen. Tech. Rep. RMRS-GTR-331. , U.S. Department of Agriculture, Forest Service, Rocky Mountain Research Station. , Fort Collins, CO.
Tomback, D.F., Achuff, P., 2010. Blister rust and western forest biodiversity: ecology, values and outlook for white pines. Forest Pathology 40 (3–4), 186–225.
Varhola, A., Coops, N.C., Weiler, M., Moore, R.D., 2010. Forest canopy effects on snow accumulation and ablation: An integrative review of empirical results. Journal of Hydrology 392 (3), 219–233.
Wei, L., et al., 2016. Simulated water budget of a small forested watershed in the continental/maritime hydroclimatic region of the United States. Hydrological Processes 30, 2000–2013.
Wei, L., et al., 2014. Constraining 3-PG with a new $\delta^{13}C$ submodel: a test using the $\delta^{13}C$ of tree rings. Plant, Cell & Environment 37 (1), 82–100.
Wei, L., et al., 2019. A heuristic classification of woody plants based on contrasting shade and drought strategies. Tree Physiology 39 (5), 767–781.
Wei, L., et al., 2018. Forest productivity varies with soil moisture more than temperature in a small montane watershed. Agricultural and Forest Meteorology 259, 211–221.
Wellner, C.A., 1976. Frontiers of Forestry Research-Priest River Experimental Forest, 1911-1976.
Whitehead, P.G., Robinson, M., 1993. Experimental basin studies—an international and historical perspective of forest impacts. Journal of Hydrology 145 (3), 217–230.